

DISTANCE MEASUREMENTS FROM THE INTERNAL DYNAMICS OF GLOBULAR CLUSTERS: APPLICATION TO THE SOMBRERO GALAXY (M 104)

KATJA FAHRION¹, MICHAEL A. BEASLEY^{2,3,4}, ANASTASIA GVOZDENKO⁵, GLENN VAN DE VEN¹, KATHERINE L. RHODE⁶, ANA L. CHIES-SANTOS⁷, ANNA FERRE-MATEU^{2,3,4}, MARINA REJKUBA⁸, OLIVER MÜLLER^{9,10,11}, AND ERIC EMSELLEM⁸

¹ Department of Astrophysics, University of Vienna, Türkenschanzstraße 17, 1180 Wien, Austria

² Instituto de Astrofísica de Canarias, Calle Vía Láctea, E-38206 La Laguna, Spain.

³ Departamento de Astrofísica, Universidad de La Laguna, E-38206 La Laguna, Spain.

⁴ Centre for Astrophysics and Supercomputing, Swinburne University, John Street, Hawthorn VIC 3122, Australia.

⁵ Department of Physics, Centre for Extragalactic Astronomy, Durham University, South Road, Durham DH1 3LE, UK.

⁶ Department of Astronomy, Indiana University, 727 East Third Street, Bloomington, IN 47405, USA.

⁷ Instituto de Física, Universidade Federal do Rio Grande do Sul (UFRGS), Av. Bento Gonçalves, 9500, Porto Alegre, RS 91501-970, Brazil

⁸ European Southern Observatory, Karl-Schwarzschild-Straße 2, 85748 Garching bei München, Germany

⁹ Institute of Physics, Laboratory of Astrophysics, Ecole Polytechnique Fédérale de Lausanne (EPFL), 1290 Sauvigny, Switzerland

¹⁰ Institute of Astronomy, Madingley Rd, Cambridge CB3 0HA, UK and

¹¹ Visiting Fellow, Clare Hall, University of Cambridge, Cambridge, UK

Version September 19, 2025

Abstract

Globular clusters (GCs) are dense star clusters found in all massive galaxies. Recent work has established that they follow a tight relation between their internal stellar velocity dispersion σ and luminosity, enabling accurate distance measurements. In this work, we aim to apply this GC velocity dispersion (GCVD) distance method to measure the distance to M 104 (NGC 4594, the Sombrero galaxy). We have measured internal stellar velocity dispersions for 85 globular clusters (GCs) and one ultra-compact dwarf galaxy around M 104 using high-resolution multi-object integrated-light spectroscopy with FLAMES/GIRAFFE on the Very Large Telescope. The measured velocity dispersions range from $\sigma = 4 - 30 \text{ km s}^{-1}$, with a mean uncertainty of $\Delta\sigma = 2.5 \text{ km s}^{-1}$. For a subset of 77 GCs with V -band magnitudes and reliable velocity dispersion measurements above $\sigma > 4 \text{ km s}^{-1}$, we constructed the M_V - σ relation to measure the distance to M 104, finding $D = 9.00 \pm 0.29$ (stat.) ± 0.26 (sys.) Mpc. The GCs follow the Milky Way and M 31 $M_V - \sigma$ relation closely, with the exception of the luminous ultra-compact dwarf SUCD1, which is nearly one magnitude brighter than the mean relation. 29 GCs in the sample have sizes determined from *Hubble* Space Telescope imaging which allowed us to determine their masses and V -band dynamical mass-to-light ratios (M/L_V). We find a mean $\langle M/L_V \rangle = 2.6 \pm 0.8 M_\odot/L_\odot$ for the luminous ($M_V < -8$ mag) M 104 GCs, which is higher than the Milky Way GCs, but is reminiscent of the brightest GCs in Centaurus A. With the exception of SUCD1, the GCs of M 104 follow the GCVD relation irrespective of their mass-to-light ratio.

Subject headings: galaxies:distances – galaxies:star clusters – galaxies:M104

1. INTRODUCTION

Globular clusters (GCs) are overall ancient star clusters found in all massive galaxies (Brodie & Strader 2006; Beasley 2020). With stellar masses $M_* = 10^4 - 10^6 M_\odot$ and compact sizes ($r_h = 2 - 10 \text{ pc}$), they are dense enough to have survived for billions of years. Consequently, as some of the oldest stellar structures in the Universe, GCs have long been employed as ancient fossils of galaxy formation and assembly.

In the Milky Way, spatially resolved studies have placed constraints on the chemical and kinematic properties of individual stars within GCs. For decades it has been known that GCs follow a tight relation between their magnitudes (or masses) and internal velocity

dispersions σ (Pryor & Meylan 1993). Similar to the Faber-Jackson relation for elliptical galaxies (Faber & Jackson 1976), this relation is a projection of the fundamental plane that arises from the Virial Theorem (Djorgovski 1995; Strader et al. 2009). However, as old stellar systems with a simple dynamical nature reflected in a narrow range of mass-to-light ratios (1 - 3; McLaughlin 2000; Baumgardt & Hilker 2018), the GC $M_V - \sigma$ relation shows remarkably small scatter. As already discussed by Paturel & Garnier (1992), Djorgovski (1995), and Strader et al. (2009), this tight relation between GC magnitudes and velocity dispersion can be employed as an accurate distance indicator.

Recently, Beasley et al. (2024) revisited the GC velocity dispersion (GCVD) distance relation by collecting V -band magnitudes and velocity dispersions for GCs in the Milky Way and M 31 (Baumgardt & Hilker 2018;

Strader et al. 2011) in order to recalibrate the relation using geometric distances derived from Gaia parallaxes. By then applying the GCVD relation to Centaurus A using 57 GCs with velocity dispersion measurements from Dumont et al. (2022), Beasley et al. (2024) demonstrated that this method can yield distances with uncertainties as low as 3 – 5%. Even more recently, the GCVD method was applied to derive a distance to the ultra diffuse galaxy NGC 1052-DF2, achieving an uncertainty of $\sim 7\%$ based on 5 GCs (Beasley et al. 2025).

As of now, application of the GCVD distance method is limited by the availability of velocity dispersion measurements. Outside the Local Group, dispersion measurements are rare as they rely on moderately high spectral resolution ($R > 10,000$) to measure dispersions down to $\sigma \sim 4 \text{ km s}^{-1}$, a typical value for a GC with a mass of $M \sim 10^5 M_{\odot}$ (the approximate mean mass of GCs in the Milky Way, Baumgardt et al. 2020). In an ongoing effort to collect larger samples of GC velocity dispersions, we present here velocity dispersions of 85 GCs and one ultra-compact dwarf galaxy (UCD) around M 104 (NGC 4594, the Sombrero galaxy), based on high-resolution spectroscopy with the FLAMES GIRAFFE multi-object spectrograph at the Very Large Telescope (VLT). In Fahrion et al. (2025), we presented an extensive catalogue of GC velocities using the same dataset combined with spectra from the OSIRIS instrument at the Gran Telescopio Canarias (GTC) and analysis of archival VLT MUSE data. In this paper, our focus is on deriving a GCVD distance to M 104. Additionally, for a subsample of 29 GCs with available size measurements, we derive dynamical masses and mass-to-light ratios.

M 104 is a particularly interesting target for the GCVD method. As a peculiar galaxy with its prominent, almost edge-on disc, M 104 has been studied extensively using space- and ground-based facilities (e.g. Emsellem 1995; Harris et al. 2010; Jardel et al. 2011; Gadotti & Sánchez-Janssen 2012; Cohen et al. 2020). Also, its rich GC system has been the focus of many studies (e.g. Wakamatsu 1977; Harris et al. 1984; Bridges & Hanes 1992; Bridges et al. 1997; Forbes et al. 1997; Larsen et al. 2002; Rhode & Zepf 2004; Bridges et al. 2007; Alves-Brito et al. 2011; Dowell et al. 2014; Kang et al. 2022). The total number of GCs is estimated to lie between 1500 and 2000 (Rhode & Zepf 2004; Kang et al. 2022), and combining literature samples with newly collected data, we collected line-of-sight velocities for 499 of those in Fahrion et al. (2025), corresponding to approximately 25% of the total GC system. With such a rich GC system, M 104 is therefore an ideal target to apply the GCVD method and test it against other distance measurements.

Distance measurements to M 104 from the literature range between ~ 7 and 22 Mpc¹ and encompass a variety of different distance indicators. Using the tip of the red giant branch (TRGB) in deep *Hubble* Space Telescope (HST) observations, McQuinn et al. (2016) derived a distance of $D = 9.55 \pm 0.13$ (stat.) ± 0.31 (sys.) Mpc, which is the most recent precise distance measurement to M 104. Older distance measurements using surface brightness fluctuations (SBF) based on infrared HST observations, Jensen et al. (2003) reported a distance of 9.08 Mpc, similar to other SBF measurements (Ciardullo

et al. 1993; Ferrarese et al. 2000; Tonry et al. 2001) that found distances between 8 and 10 Mpc. Similar values were also reported based on the luminosity functions of GCs (GCLF; Bridges & Hanes 1992; Spitler et al. 2006) and planetary nebulae (PNLF; Ciardullo et al. 1993; Ford et al. 1996).

The aim of this paper is to construct the GCVD relation for M 104 GCs for a precise distance measurement. The paper is structured as follows: In Sect. 2, we describe the FLAMES high-resolution data. Sect. 3 describes our methods of measuring dispersions and correcting for aperture effects. The distance measurement is detailed in Sect. 5 and Sect. 4 describes the mass-to-light ratios for a subsample of GCs. We summarise and conclude in Sect. 7.

2. DATA

The GC system of M 104 was observed with FLAMES in January and February 2025 (Programme ID 114.274W, PI: Fahrion). We used the FLAMES instrument with the GIRAFFE spectrograph fed by 135 MEDUSA fibers deployed over the field of view (25' diameter). With two pointings, north and south of the disc, we placed MEDUSA fibers on 221 GC candidates; 93 of them could be identified as GCs bound to M 104. SUCD1, a previously identified UCD was also included (Hau et al. 2009).

Full details of the observations and data reduction are given in Fahrion et al. (2025). To summarise, we used the FLAMES GIRAFFE HR21 (875nm) grating, which provides coverage of the calcium triplet region from 8483 to 8900 Å with resolution of $R = 18,000$ and sampling of $0.05 \text{ \AA pix}^{-1}$. Each pointing was covered in ten exposures of 1365 seconds each, distributed over five observing blocks. Targets were selected from the catalogues of Spitler et al. (2006), Harris et al. (2010) and Kang et al. (2022).

The data were reduced using standard procedures using the FLAMES GIRAFFE ESOREX pipeline and custom scripts, with the variation that the sky-subtraction was performed using PXP (Cappellari & Emsellem 2004; Cappellari 2017, 2023) to fit each spectrum with a stellar model from the PHOENIX library (Husser et al. 2013) and sky templates as sky input. After sky subtraction, spectra from individual exposures were corrected for barycentric velocities, resampled, and combined using a median weighted by the signal-to-noise (S/N) ratio of each spectrum.

We also kept a version of spectra with sky lines for masking purposes (see below). Additionally, we used those to test the final spectral resolution of our spectra by fitting prominent sky lines with Gaussian curves. We found a median full width at half maximum (FWHM) of the sky lines of $0.54 \pm 0.04 \text{ \AA}$. and did not observe any variation in the spectral resolution with wavelength.

3. METHODS

In the following, we describe our methods to derive velocity dispersions from the FLAMES spectra. Additionally, we describe the available photometry and how mass-to-light ratios were derived. Sect. 5 then details the distance measurements.

3.1. Spectral fitting

¹ From the NASA/IPAC Extragalactic Database

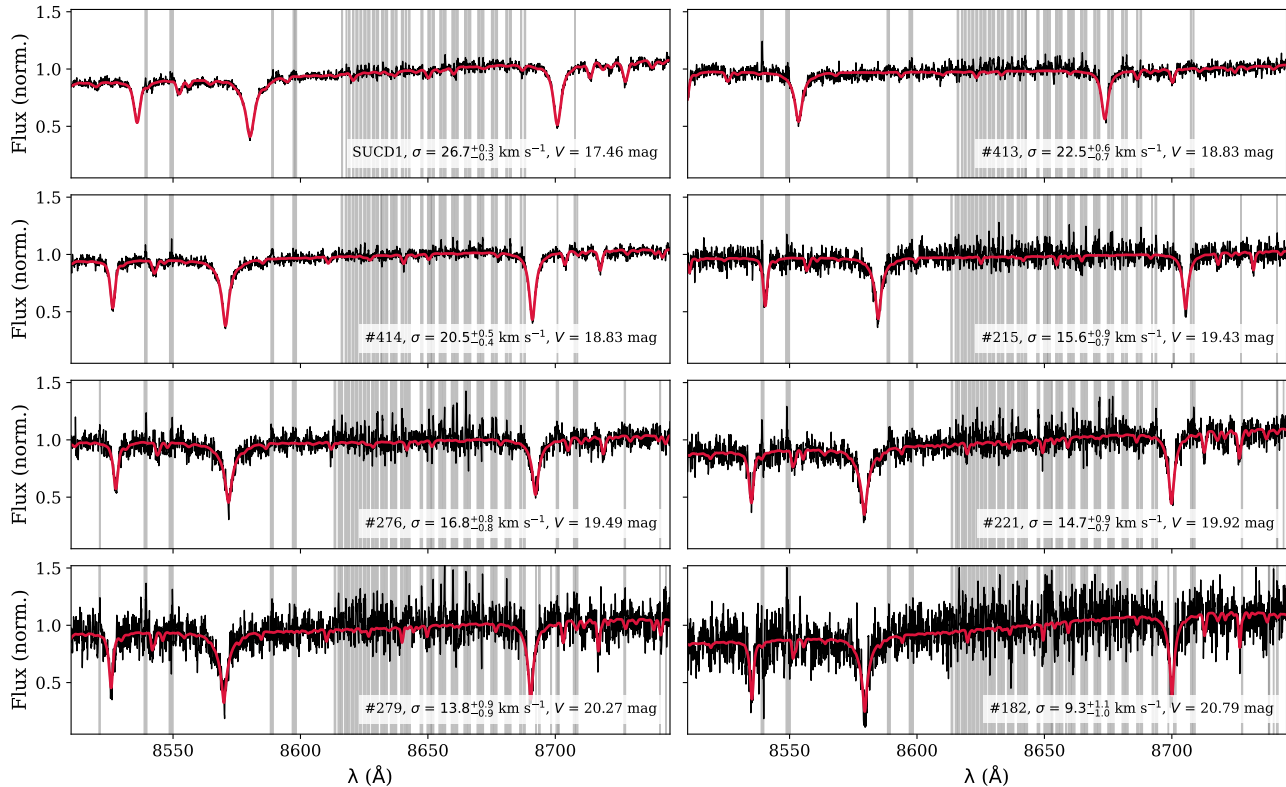


FIG. 1.— Examples of FLAMES GC spectra. Original spectrum in black, pPXF fit in red. The grey regions indicate the positions of sky lines which were masked out before performing the fits. The GC identifier and the best-fitting velocity dispersion (before aperture correction) are noted in the bottom right corner of each panel.

We fit the FLAMES GC spectra with pPXF (Cappellari & Emsellem 2004; Cappellari 2017, 2023). pPXF fits the spectrum with a library of suitable model or empirical spectra and returns the parameters of the line-of-sight velocity distribution (LOSVD) such as radial velocity and velocity dispersion. We chose additive polynomials of degree 4 and multiplicative polynomials of degree 1 to account for variations in the continuum and flux calibrations, but as described in Beasley et al. (2025), the results are not very sensitive to the choice of degree of the polynomials. Because sky residuals remained in the reduced data, we carefully masked those lines using a custom mask for every spectrum. We began by normalising the spectrum without sky subtraction in a continuum wavelength range to the continuum level of the sky-subtracted spectrum. Then, we masked out all wavelength pixels in which the normalised sky spectrum exceeds 1.2 times the continuum level. We fitted all spectra in a wavelength range between 8450 and 8850 Å except for four GCs that had strong sky residuals at redder wavelengths. Here, we restricted the upper wavelength range to 8750 Å due to strong sky residuals at longer wavelengths.

We used the high-resolution stellar population models from Coelho (2014) to fit the FLAMES spectra. In a first step, we selected red (sub) giant stars with effective temperature between 4500 and 5000 K, surface gravity between $\log(g)=2.0$ and 4.0, and metallicities between -1.5 and 0 dex. Then, the selected model spectra were brought to a spectral resolution of 0.54 Å to match the FLAMES spectra. Figure 1 shows eight GC spectra and their fits as examples.

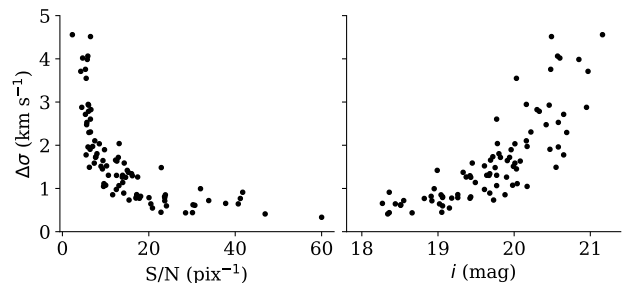


FIG. 2.— Symmetric velocity dispersion uncertainty as a function of spectral signal-to-noise (left) and i -band magnitude (right).

As described in Fahrion et al. (2025), we performed a Monte-Carlo approach to obtain random uncertainties. For this, 100 representations of the input spectrum were created by drawing values from the residual of the initial fit and adding it onto the initial best fit spectrum. These 100 spectra were then fitted with pPXF for bootstrapping. We used the corresponding histograms of line-of-sight velocities and dispersions to derive the best-fit values and their uncertainties as the 16th, 50th, and 84th percentiles of the distributions. We show the resulting uncertainties on the velocity dispersion as a function of spectral signal-to-noise (S/N) and GC i -band magnitude (from Kang et al. 2022) in Fig. 2. From the full sample of 93 GCs, 85 have velocity dispersion uncertainties below 5 km s⁻¹ and dispersions $\sigma > 4$ km s⁻¹. For the distance measurements, we considered this sample of 85 GCs with reliable velocity dispersion measurements ($\sigma > 4$ km s⁻¹, $\Delta\sigma < 5$ km s⁻¹).

3.2. Aperture Corrections

The FLAMES velocity dispersions are measured through a finite fibre aperture ($1.2''$) and therefore may differ from the true GC velocity dispersions due to incomplete sampling of the GC light. This can occur because light from the outer regions of the cluster may fall outside the fibre, or light from the central regions of the GC is missed due to uncertainties in fibre centering due to either mechanical or astrometrical uncertainties. These effects were explored in detail in [Beasley et al. \(2025\)](#) where the dual impacts of light falling outside the aperture and imperfect centring on velocity dispersion as a function of seeing, GC size, and distance were simulated.

For the sizes of M104 GCs (~ 3.5 pc; [Spitler et al. 2006; Harris et al. 2010](#)), seeing conditions of our observations ($\sim 1''$) and at the distance of M104 ($D \sim 10$ Mpc; [McQuinn et al. 2016](#)) we find that our observations typically underestimate the true GC dispersions by $\sim 0.4\%$. This effect is dominated by centring uncertainties of the FLAMES fibres. The exception to this is SUCD1, which is sufficiently large to lose some low dispersion light from its outer regions and, in this case our measured dispersion overestimates the true value by $\sim 0.4\%$. While these are small effects, they do have a minor impact on distances measured by the GCVD method. Therefore, where sizes are available we calculate and apply aperture corrections on a cluster by cluster basis. Where no size information is available, we apply a correction based on the average GC size.

We give the full sample of velocity dispersion measurements in Appendix A. The values range between 4 and 30 km s^{-1} with mean uncertainties of $\sim 2.5 \text{ km s}^{-1}$. For SUCD1, we measured an aperture-corrected dispersion of $\sigma = 26.6 \pm 0.3 \text{ km s}^{-1}$, in agreement with the measurement by [Hau et al. \(2009\)](#) of $\sigma = 25.0 \pm 5.6 \text{ km s}^{-1}$ based on a lower resolution Keck/DEIMOS spectrum.

3.3. Available photometry

To directly apply the GCVD approach using the relation calibrated on Local Group GCs, V -band magnitudes are needed. For our sample of 85 GCs (not including SUCD1) with velocity dispersion uncertainties $< 5 \text{ km s}^{-1}$ and velocity dispersions $\sigma > 4 \text{ km s}^{-1}$, 29 have high quality B, V, R -band magnitudes available from imaging with the Advanced Camera for Surveys (ACS) onboard HST data ([Spitler et al. 2006; Harris et al. 2010](#)).

Moreover, 68 GCs have B, V, R -band magnitudes available from [Rhode & Zepf \(2004\)](#) based on imaging with the Mosaic detector on the Kitt Peak 4 metre telescope. The ones with V -band magnitudes available from both studies show good agreement within 0.1 mag. In total, V -band magnitudes are available for 77 of 85 suitable GCs, in a magnitude range of $V \sim 19 - 22$ mag. For SUCD1, [Hau et al. \(2009\)](#) reported a V -band magnitude of 17.46 mag based on the same HST/ACS observations as used by [Spitler et al. \(2006\)](#) and [Harris et al. \(2010\)](#). In addition, all GCs have u, g, i -band magnitudes from [Kang et al. \(2022\)](#) available, based on CFHT/MegaCam imaging.

Figure 3 shows the relation between velocity dispersion and apparent magnitudes in different filters. In all cases, a strong relationship is found due to the underlying relation between mass and dispersion. As the GCVD

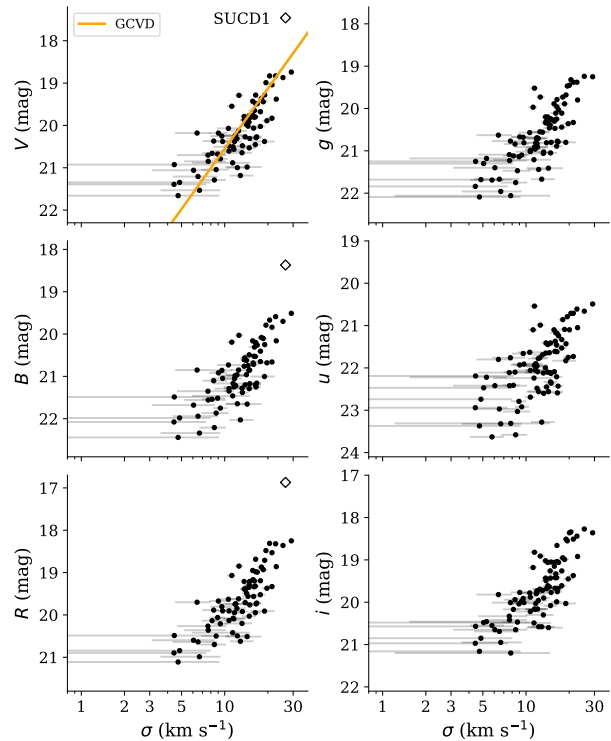


FIG. 3.— Velocity dispersions versus apparent magnitudes in different filters. The orange line shows the GCVD relation at a distance of 9.00 Mpc.

relation is currently only calibrated on V -band magnitudes (shown in the top left panel), we show here the other filters only for visualisation. In Sect. 5 we also explore distance measurements based conversions from g and i to V -band magnitudes.

4. MASS-TO-LIGHT RATIOS

For a subsample of 29 GCs and SUCD1, size measurements are available based on HST imaging ([Hau et al. 2009; Harris et al. 2010](#)). We derive V -band mass-to-light ratios (M/L_V) using the aperture-corrected global velocity dispersions (σ_{gl}) and half-light radii (r_h). We obtain virial masses for the Sombbrero GCs from Eq. 1 (e.g. [Larsen et al. 2002; Beasley et al. 2025](#)):

$$M_{\text{dyn}} = 10 \frac{\sigma_{\text{gl}}^2 r_h}{G} \quad (1)$$

[Beasley et al. \(2025\)](#) showed that Eq. 1 yields good agreement with M_{dyn}/L_V values determined for Milky Way GCs using spatially resolved stellar dispersion profiles. Therefore, M_{dyn}/L_V determined via Eq. 1 (e.g. also for the M31 GCs from [Strader et al. 2011](#) and Cen A data from [Dumont et al. 2022](#)) and M_{dyn}/L_V measured for the Milky Way GCs should be directly comparable.

The derived mass-to-light ratios are shown in Fig. 4 compared to GCs around Centaurus A ([Dumont et al. 2022](#)), M31 ([Strader et al. 2011](#)), and the Milky Way ([Baumgardt et al. 2020](#)). The values are colour-coded according to their metallicities, derived from the FLAMES spectra (see [Fahrion et al. 2025](#)). We also included a line marking the mean of the MW GCs ($\langle M/L_V \rangle_{\text{MW}} = 1.77 \pm 0.1 M_{\odot}/L_{\odot}$, [Beasley et al. 2025](#) based on data from [Baumgardt et al. 2020](#)).

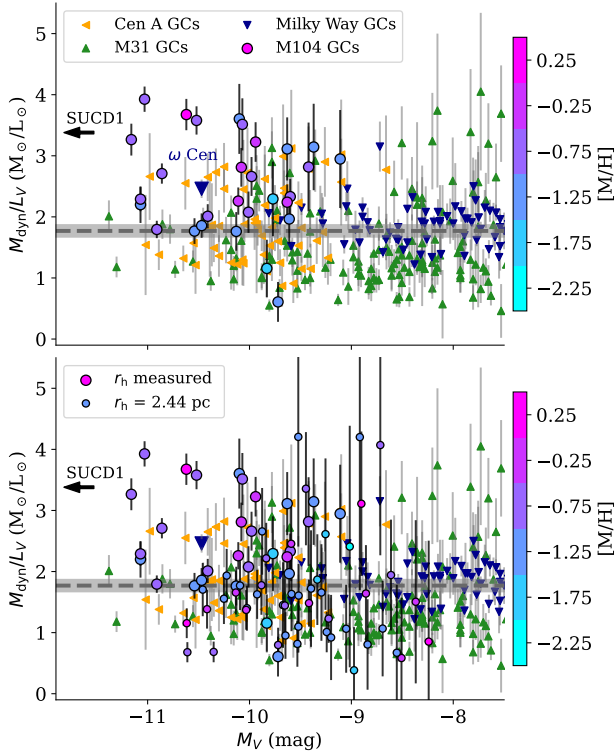


FIG. 4.— Mass-to-light ratios for the M104 GCs in comparison with GCs around Centaurus A (Dumont et al. 2022), M31 (Strader et al. 2011), and the Milky Way (Baumgardt et al. 2020). The M104 GCs are colour-coded according to their metallicity. SUCD1 is outside the plotted x-range at $M_V = -12.44$ mag, indicated by the arrow. The dashed grey line indicates the mean of the Milky Way GCs. ω Centauri (NGC 5139) is marked by the larger blue symbol. In the bottom panel, we show the full sample of GCs with dispersion measurements and V -band magnitudes, assuming a half-light radius of $r_h = 2.44$ pc, where no size measurements are available.

We find M_{dyn}/L_V values in a range from $\sim 1 - 4M_{\odot}/L_{\odot}$, with a mean $\langle M/L_V \rangle = 2.6 \pm 0.8M_{\odot}/L_{\odot}$ for this sample of M104 GCs. Many of them have higher mass-to-light ratios than the MW population, but they are also considerably brighter than most of the Galactic GCs. The brightest M104 GCs are even significantly brighter than ω Centauri, the most massive GC of the Milky Way, that also shows an increased mass-to-light ratio.

We find reasonable agreement with GCs in Centaurus A ($\langle M/L_V \rangle_{\text{Cen A}} = 2.0 \pm 0.9M_{\odot}/L_{\odot}$), but a direct comparison is difficult based on the low number of size measurements available for our M104 sample. Similar to the behaviour seen in the Centaurus A GCs (Dumont et al. 2022), we also observe a range in mass-to-light ratio that exceeds those of the Milky Way GCs ($M/L \sim 1.5$). From their analysis, Dumont et al. (2022) interpreted this scatter with a population of stripped nuclei masquerading as GCs. In M104, we find that SUCD1 indeed shows an elevated mass-to-light ratio, in line with other UCDs (e.g. Rejkuba et al. 2007; Mieske et al. 2008). Nonetheless, the defining feature that sets it apart from the GC population is its significantly larger luminosity, being about 1.4 magnitudes brighter than the next brightest GC. Based on its magnitude, size, and velocity dispersion, we derive a dynamical mass of $M_{\text{dyn}} = (2.4 \pm 0.2) \times 10^7 M_{\odot}$, similar to the value reported

by Hau et al. (2009).

In the lower panel of Fig. 4, we also included GCs that lack direct size measurements. For those, we assumed a size of 2.44 pc, corresponding to the median of size measurements as reported in Harris et al. (2010). These estimated M/L_V values show a similar range, with several GCs having similar values as Milky Way GCs. However, we note that the uncertainties increase substantially for the fainter GCs.

5. DISTANCE TO SOMBRERO

We obtained a distance to Sombrero using the GCVD approach, which is based on the fact that GCs in the Local Group obey a tight $M_V - \sigma_{\text{gl}}$ relation and on the assumption that extragalactic GC systems also follow this relation. See Beasley et al. (2024) and Beasley et al. (2025) for full details of the technique and systematic uncertainties.

5.1. Distance measurement with the GCVD relation

We used the same approach as that used in Beasley et al. (2024, 2025) and fit the relation between apparent V -band magnitudes and velocity dispersions σ with a log-linear relation of the form:

$$V = \beta_0 + \beta_1 \log_{10}(\sigma), \quad (2)$$

where β_1 is the slope of the relation and β_0 describes the offset. In Beasley et al. (2024), the relation was calibrated based on Milky Way and M31 GCs, giving values of $\beta_{0,\text{calibrated}} = -4.49 \pm 0.04$ and $\beta_{1,\text{calibrated}} = -4.73 \pm 0.05$. Therefore, when using a fixed slope, the derived offset scales with the distance modulus μ :

$$\mu = \beta_{0,\text{measured}} - \beta_{0,\text{calibrated}} \quad (3)$$

As described in Beasley et al. (2025), we fit the apparent V -band magnitudes and velocity dispersions using a Markov Chain Monte Carlo (MCMC) ensemble sampler (EMCEE; Foreman-Mackey et al. 2013) to determine β_0 and its uncertainties. We used a Gaussian likelihood function that includes uncertainties in V and σ . For the offset, we chose a uniform prior in the range of $-10 < \beta_0 < 31$ (corresponding to distances from the Milky Way out to 100 Mpc). 25 walkers and 10000 chains were used and the corresponding distances describe the median of the posterior distribution with the 16th and 84th percentiles as lower and upper uncertainties. Due to the limited range in magnitudes, we kept the slope fixed to the calibrated relation. In future work, we aim to test the universality of the slope with a larger sample of GC velocity dispersions.

5.1.1. Distances from different samples

Distance results based on differing photometric samples are presented in Table 1. We can explore the reliability of the GCVD method by dissecting the full GC sample. For example, we can limit the GC sample to only those that have high quality HST-based Johnson V -band magnitudes available. Both Spitler et al. (2006) and Harris et al. (2010) provide V -band magnitudes based on the same HST/ACS imaging that comprises a 6-pointing mosaic of Sombrero. Overall the photometry from the two studies is in reasonable agreement, although there are

TABLE 1
DISTANCE ESTIMATES TO SOMBRERO FROM DIFFERENT PHOTOMETRIC SAMPLES

Photometry	Distance \pm stat. error (Mpc)	No. GCs
Combined V-band	9.00 ± 0.29	77
Spitler et al. (2006)	9.33 ± 0.32	29
Harris et al. (2010)	9.00 ± 0.33	29
Rhode & Zepf (2004)	8.89 ± 0.30	68
V predicted from g (Kang et al. 2022)	9.03 ± 0.30	85
V predicted from i (Kang et al. 2022)	9.14 ± 0.29	85

TABLE 2
SOURCES OF SYSTEMATIC UNCERTAINTY

Source	Uncertainty (Mpc)
Aperture/positioning error	0.03 (0.2%)
Different photometric samples	0.16 (1.7%)
Different M_{dyn}/L_V	0.20 (2.2%)

differences in the final magnitudes due to different approaches in the aperture correction. Spitler et al. (2006) used a fixed value for all sources, while Harris et al. (2010) used size-dependent aperture corrections. While we have no specific preference for the photometry from either source, the photometry from Harris et al. (2010) might be more reliable as it takes the GC sizes into account and is based on a more detailed consideration of the point spread function that was determined empirically with proximal stars on a cluster-by-cluster basis. There are 29 GCs (excluding SUCD1) in our spectroscopic sample that overlap with both these data sets. For the photometry from Spitler et al. (2006), we measure $D = 9.33 \pm 0.32$ Mpc, while for the Harris et al. (2010) photometry, we obtain $D = 9.00 \pm 0.33$ Mpc.

We also matched V -band photometry from the ground-based study of Rhode & Zepf (2004) with our sample, yielding 68 GCs. Rhode & Zepf (2004) adopted a single value for the extinction correction of $A_V = 0.171$, while Spitler et al. (2006) adopted $A_V = 0.163$. We therefore adjusted the Rhode & Zepf (2004) V -band magnitudes by -0.008 mag to match the Spitler et al. (2006) and Harris et al. (2010) photometry.

For this sample we obtain $D = 8.89 \pm 0.30$ Mpc. Therefore, all three samples give similar results, with a standard deviation of only 0.16 Mpc. In view of this, we combined the three samples taking the average of the V -band magnitudes in the cases where more than one measurement was available. For this combined sample of 77 GCs, we find $D = 9.00 \pm 0.29$ Mpc, which we adopt as our fiducial distance measurement.

Similarly, we can expand the sample by taking the GCs into account that have no V -band magnitudes available, but u, g, i photometry from Kang et al. (2022). To convert their g - and i -band magnitudes to V -band, we made use of the EMILES SSP models (Vazdekis et al. 2010, 2016). Applying the appropriate filter transmission curves for CFHT/MegaCam and Johnson V using SYNPHOT² (STScI Development Team 2018), we derived predictions for $V - i$ colours depending on the metallicity of the SSP models, assuming an age of 13 Gyr representative for typical GC systems (Beasley et al. 2008; Caldwell et al. 2011). Then, we used these predictions to convert the g - and i -band magnitudes to V -band, based

on the measured metallicities (Fahrion et al. 2025). Deriving the GCVD distance with the V -band magnitudes predicted from g -band magnitudes yields a distance of $D = 9.03 \pm 0.30$ Mpc, while applying this transformation from i - to V -band gives a distance of $D = 9.14 \pm 0.29$ Mpc, verifying the validity of the colour conversion.

5.1.2. Systematics

We explored the impact of systematic effects on our distances by considering three key sources of systematic uncertainty: the impact of aperture corrections and fibre centring errors, the effect of using photometry from different sources and samples, and the impact of varying M_{dyn}/L_V . A summary is found in Table 2.

The effect of aperture and fibre centering on the velocity dispersion measurement is discussed in Sect. 3.2. These corrections translate to a uncertainty on our distances of 0.03 Mpc (0.2%) (i.e., this is the difference in distance we obtain with GCVD between the measured velocity dispersions and the aperture-corrected dispersions). Similarly, the impact of different photometry and photometric samples is discussed in Sect. 5.1.1, from which we obtain a standard deviation on the three different distances of 0.16 Mpc (1.7% distance uncertainty).

To investigate the impact of varying M_{dyn}/L_V on GCVD, we used the sizes from Harris et al. (2010) where available. To also include the remaining sample, we assumed for the other GCs a mean size of 2.44 pc, the mean of the size measurements (see Sect. 4). We then performed bootstrap resampling with replacement, where we only selected GCs with $M/L_V < 3.0$ to match the Milky Way M_{dyn}/L_V and M31 distributions. In all cases the GCVD slope was fixed to the fiducial value, and we just consider the impact on the offset β_0 . As a result of this exercise, we find that the offset can shift by up to 0.2 Mpc (2.2%).

Combining the above mentioned sources of systematics corresponds to a total systematic uncertainty of ± 0.26 Mpc, or 2.9%.

5.1.3. Dependence on GC parameters

After fitting the GCVD relation to the M104 GCs, we find a scatter of the residuals of $\sim 6\%$. This is very similar to the scatter in the GC samples of the Milky Way, M31, and Centaurus A (see Fig. 5) and suggests that this scatter is intrinsic to such GC samples. In Fig. 6, we colour-coded the GCs according to different parameters to test if the scatter correlates with GC parameters.

In the left panel of Fig. 6, the GCs are colour-coded according to their metallicity. The metallicity values are drawn from the full M104 sample described in Fahrion et al. (2025). Where available, we used metallicities from optical VLT/MUSE or GTC/OSIRIS spectroscopy, and

² <https://synphot.readthedocs.io/en/latest/>

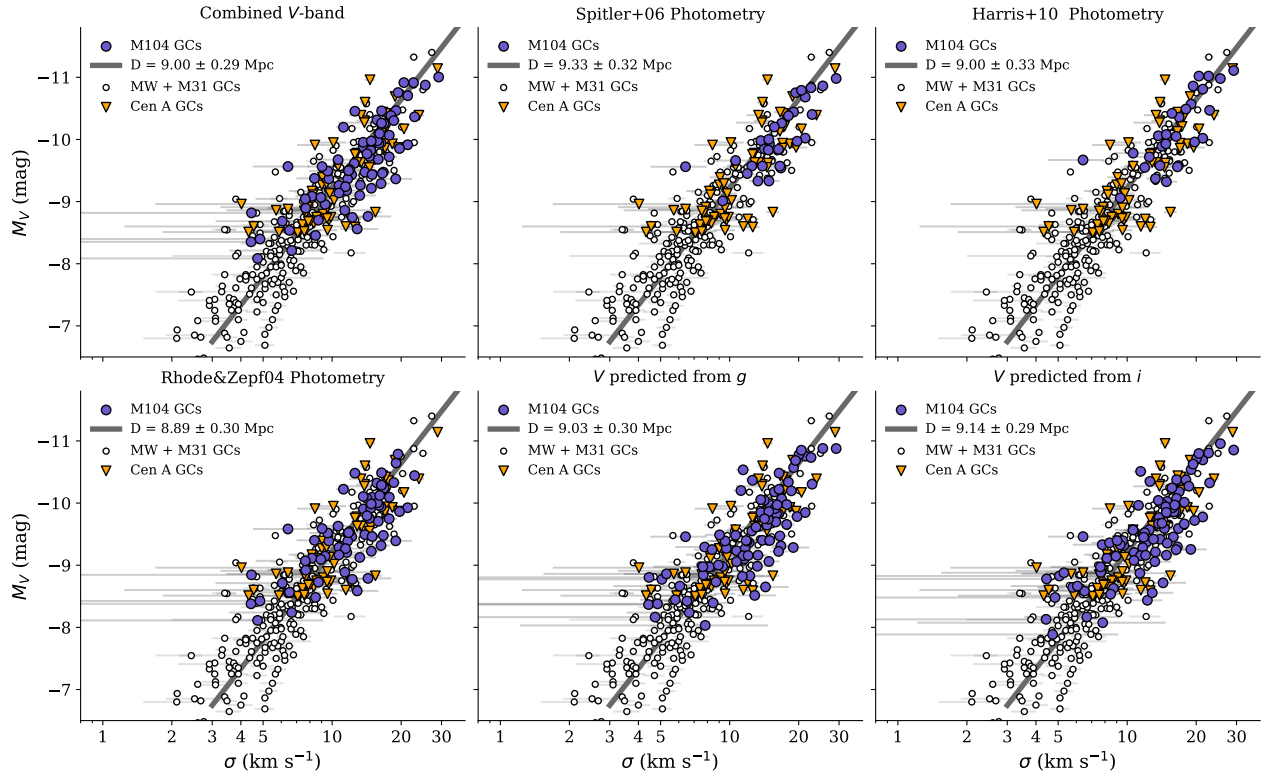


FIG. 5.— Relationship between absolute V -band magnitude and velocity dispersion for the M104 GCs based on different photometric samples. From top left to bottom right: Combined V -band photometry, photometry from Spitler et al. (2006) and Harris et al. (2010) based on HST observations, ground-based photometry from Rhode & Zepf (2004), and V -band magnitudes predicted from the ground-based g and i photometry presented by Kang et al. (2022). The solid line in each panel indicates the GCVD relation at the best-fitting distance. White circles show GCs from the Milky Way and M31, orange triangles are GCs around Centaurus A (Beasley et al. 2024).

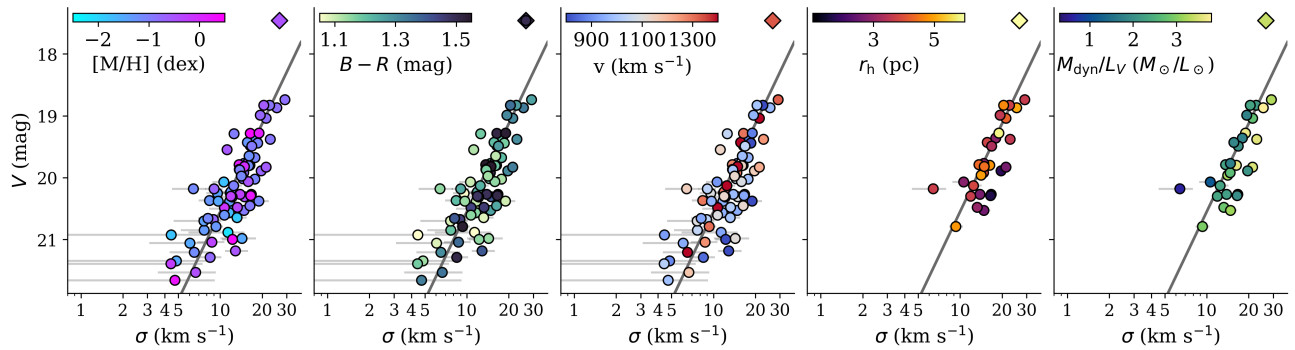


FIG. 6.— Relationship between apparent magnitude and velocity dispersion, colour-coded with different properties. From left to right: metallicities, $B - R$ colours, line-of-sight velocities, half-light radii, and mass-to-light ratios. The solid line is the GCVD relation at a distance of 9.0 Mpc.

for the remaining GCs the metallicities were derived directly from full spectrum fitting to the FLAMES spectra. While the GCs with measured dispersions cover a broad range of metallicities, there seems to be no clear correlation with the scatter in the magnitude-dispersion plane. Splitting the MW and M31 GCs into metal-poor and metal-rich GCs, Beasley et al. (2024) found no difference in the GCVD relation’s slope or offset, in agreement with our finding for M104.

Similarly, there seems to be no clear correlation between the $B - R$ colour and the scatter on the GCVD relation, as the second panel of Fig. 6 shows. Also, the scatter does not seem to correlate with the line-of-sight velocity of the GCs.

The fourth panel shows GCs with available size measurements. There might be a hint that smaller-sized GCs lie to the right of the GCVD relation, but this is driven by three objects and a larger sample is required to test this dependence. However, the observed offset of SUCD1 could be explained by the size difference as it is a particularly large object with a reported half-light radius of $r_h = 14.7 \pm 1.4$ pc (Hau et al. 2009), significantly larger than typical GCs (mean $r_h \sim 2 - 3$ pc, Harris et al. 2010; Masters et al. 2010). As the GCVD relation is a consequence of the Virial Theorem, based on the relation between total mass and the combination of velocity dispersion squared and size ($\sigma^2 R_h$), the size can influence the position of a source on the relation, with the effect

expected to scale linearly. With the much larger size of SUCD1, this effect might play a role, while the narrow range of GC sizes does not have a large impact.

The final panel in Fig. 6 shows the GCs colour-coded by their dynamical mass-to-light ratio as described in the following section. GCs with larger mass-to-light ratios appear to lie preferentially to the right of the GCVD relation. Given that the dynamical mass scales with the square of the velocity dispersion, this is perhaps not surprising, but indicates that the GCVD distance method might only be applicable for objects within a narrow range of mass-to-light ratios. Interestingly, SUCD1 is an outlier in this respect as it lies above the relation, but still has a larger mass-to-light ratio than most of the GCs (see Sect. 4). This is likely a consequence of the elevated mass-to-light ratio of SUCD1 stemming from its large size, while the higher mass-to-light ratios of the GCs are driven by an increased velocity dispersion.

6. COMPARISON TO LITERATURE DISTANCES

As a well studied galaxy, multiple distance measurements to M 104 exist with varying accuracy. As described in Sect. 1 and discussed by McQuinn et al. (2016), distances to M 104 vary between ~ 7 and 22 Mpc, with the more accurate measurements placing the galaxy between 8 and 10 Mpc (e.g. Jensen et al. 2003; Spitler et al. 2006; McQuinn et al. 2016). McQuinn et al. (2016) note that distance measurements for M 104 based on the Tully-Fisher relation generally find larger distances, between $\sim 11 - 22$ Mpc (Bottinelli et al. 1984; Tully & Fisher 1988; Sorce et al. 2014). This may be due to the peculiar morphology and spatially restricted gas distribution of M 104 that make the morphological classification of this galaxy somewhat uncertain, and set it apart from more typical elliptical and spiral galaxies.

In Fig. 7, we show distances from the literature in comparison with our fiducial GCVD distance of $D = 9.00 \pm 0.29$ Mpc from fitting the combined V -band magnitudes (see Sect. 5). As can be seen from this figure, the GCVD distance compares well against literature measurements from various sources. For example, the median of the shown GCLF, PNLF, SBF, and TRGB distances is at 9.25 Mpc, and calculating the weighted mean taking the statistical uncertainties into account, we find $\langle D \rangle = 9.09 \pm 0.08$ Mpc, with a dispersion of 0.60 Mpc.

We find that the GCVD distance agrees very well with the PNLF distances reported by Ciardullo et al. (1993), Ford et al. (1996), and Ferrarese et al. (2000) that are all based on the dataset collected by Ford et al. (1996). While Ciardullo et al. (1993) used a preliminary analysis of the PNLF at that time, Ferrarese et al. (2000) recomputed the PNLF distance after deriving a Cepheid-based calibration for PNLF and other distance indicators. A similar Cepheid-based calibration was used for their SBF distance, based on HST imaging obtained with the wide field planetary camera 2 (WFPC2) described in Ajhar et al. (1997) and later used in Tonry et al. (2001). Jensen et al. (2003) used new HST Near Infrared Camera and Multi-Object Spectrometer (NICMOS) data for their SBF distance measurement, which is also in agreement with the GCVD distance.

While most distances agree with our GCVD distance within 1σ of the combined statistical uncertainties, there are exceptions. For example, the GCLF distance of

$D = 8.0 \pm 0.2$ Mpc reported by Spitler et al. (2006) would place the Sombrero galaxy significantly closer than our GCVD distance. As Spitler et al. (2006) discuss, assuming a distance of 9.0 Mpc would make the turnover magnitude of the GCLF about 0.3 mag brighter than the universally adopted value. However, investigation of early-type galaxies in the Virgo and Fornax galaxy clusters have found that massive galaxies often have brighter GCLF turnover magnitudes (by $\sim 0.1 - 0.3$ mag compared to low-mass galaxies, Villegas et al. 2010). The bright turnover magnitude in M 104 might therefore be a consequence of M 104 being a massive galaxy ($M_* \sim 2 \times 10^{11} M_\odot$ Jardel et al. 2011; Karunakaran et al. 2020).

Comparing the GCVD relation to the TRGB distance of $D = 9.55 \pm 0.13$ Mpc from McQuinn et al. (2016) also shows an offset within 2σ , mostly due to the small statistical uncertainties of the TRGB measurement. Their precise value is based on dedicated, deep HST/ACS data, but McQuinn et al. (2016) quote a systematic uncertainty of ± 0.31 Mpc stemming from the TRGB calibration (Carretta et al. 2000; Rizzi et al. 2007). Under consideration of this systematic uncertainty, the TRGB and GCVD distances agree. Sabbi et al. (2018) also derived a TRGB distance to M 104 based on HST Wide Field Camera 3 (WFC3) data and they found a larger distance of $D \sim 10$ Mpc. However, given that their data is shallower, they caution that the location of the TRGB is not clearly detected in their data. In the future, additional observations with JWST could be used to measure precise TRGB and SBF distances (e.g. Anand et al. 2024; Jensen et al. 2025).

7. CONCLUSIONS

In this paper, we employed the relationship between GC luminosities and their internal velocity dispersions to derive the distance to M 104 using the GCVD relation. We summarise our findings as follows:

- Using FLAMES high resolution spectroscopy, we derived velocity dispersions of 93 GCs and one UCD. Of those, 85 GCs have $\sigma > 4$ km s $^{-1}$ and velocity dispersion uncertainties < 5 km s $^{-1}$, which we used to derive the GCVD-based distance.
- Using V -band magnitudes from space- and ground-based observations of 77 GCs, we applied the GCVD relation with fixed slope and obtained a distance of $D = 9.00 \pm 0.29$ (stat.) ± 0.26 (sys.) Mpc. We find an intrinsic scatter of $\sim 6\%$. Testing different photometric samples including V -band magnitudes derived from other filters finds consistent distance measurements.
- We find that SUCD1, a known UCD near M 104, does not follow the GCVD relation and instead shows an offset. This may be related to its larger size or possibly more complex stellar population than the GCs we studied. With a reported half-light radius of 14 pc, SUCD1 is significantly larger than typical GCs.
- For a subsample of 29 GCs with available size measurements, we derived dynamical mass-to-light ratios, finding a range of values from $M_{\text{dyn}}/L_V \sim$

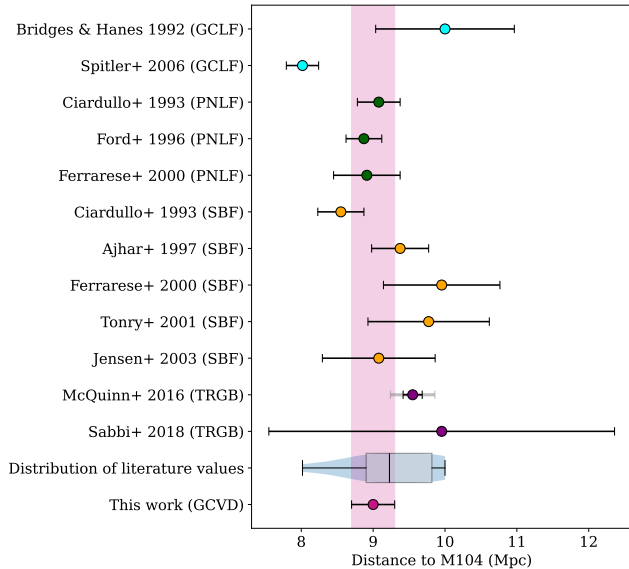


FIG. 7.— Distance measurements from the literature in comparison to the distance obtained with the GCVD method (pink point). Literature values are grouped according to the employed method. Distances from the GC luminosity function are shown in cyan (Bridges & Hanes 1992; Spitler et al. 2006), green circles refer to measurements from the planetary nebulae luminosity function (Ciardullo et al. 1993; Ford et al. 1996; Ferrarese et al. 2000), SBF distances are shown in orange (Ciardullo et al. 1993; Ajhar et al. 1997; Ferrarese et al. 2000; Tonry et al. 2001; Jensen et al. 2003), and TRGB distances from in purple (McQuinn et al. 2016; Sabbi et al. 2018). Black errorbars show 1σ statistical uncertainties and the light grey errorbar shows the systematic uncertainties for the TRGB distance from McQuinn et al. (2016). The box plot shows the distribution of literature distances, with the vertical black line indicating the median.

$1 - 4 M_{\odot}/L_{\odot}$. Similar values were found for GCs in the halo of Centaurus A (Dumont et al. 2022), while GCs in the Milky Way typically have lower M_{dyn}/L_V values, but also have lower masses than the studied M104 GCs. Besides SUCD1, other GCs with elevated mass-to-light ratios follow the GCVD relation.

- Our best-fitting distance of $D = 9.00 \pm 0.29$ Mpc agrees well with previous distance measurements in the literature that typically range from 8 to 10 Mpc. Our GCVD distance places M104 slightly closer than the TRGB distance of $D = 9.55 \pm 0.13$ (stat.) ± 0.31 (sys.) Mpc reported in McQuinn et al. (2016), which currently has the lowest reported statistical uncertainty but a larger systematic uncertainty. Nonetheless, the two distance measurements agree within 2σ .

With velocity dispersion measurements of 85 GCs, the sample presented here is already the second largest sample of GC velocity dispersion measurements beyond the Local Group after Centaurus A. In the future, we plan to collect additional high-resolution spectroscopy of extragalactic GC systems to explore the GCVD method, its applicability and underlying systematics with larger samples.

ACKNOWLEDGMENTS

KF acknowledges funding from the European Union’s Horizon 2020 research and innovation programme under the Marie Skłodowska-Curie grant agreement No 101103830. ACS acknowledges support from FAPERGS (grants 23/2551-0001832-2 and 24/2551-0001548-5), CNPq (grants 314301/2021-6, 312940/2025-4, 445231/2024-6, and 404233/2024-4), and CAPES (grant 88887.004427/2024-00). A.F.M acknowledges support from RYC2021-031099-I of MICIN/AEI/10.13039/501100011033/ UE NextGenerationEU/PRTR. O.M. is grateful to the Swiss National Science Foundation for financial support under the grant number PZ00P2_202104. This work made use of Astropy:³ a community-developed core Python package and an ecosystem of tools and resources for astronomy (Astropy Collaboration et al. 2013, 2018, 2022). Based on observations collected at the European Southern Observatory under ESO programme 114.274W (PI: Fahrion).

REFERENCES

- Ajhar E. A., Lauer T. R., Tonry J. L., Blakeslee J. P., Dressler A., Holtzman J. A., Postman M., 1997, *AJ*, **114**, 626
- Alves-Brito A., Hau G. K. T., Forbes D. A., Spitler L. R., Strader J., Brodie J. P., Rhode K. L., 2011, *MNRAS*, **417**, 1823
- Anand G. S., et al., 2024, *ApJ*, **973**, 83
- Astropy Collaboration et al., 2013, *A&A*, **558**, A33
- Astropy Collaboration et al., 2018, *AJ*, **156**, 123
- Astropy Collaboration et al., 2022, *ApJ*, **935**, 167
- Baumgardt H., Hilker M., 2018, *MNRAS*, **478**, 1520
- Baumgardt H., Sollima A., Hilker M., 2020, *PASA*, **37**, e046
- Beasley M. A., 2020, in , *Reviews in Frontiers of Modern Astrophysics; From Space Debris to Cosmology*. pp 245–277, doi:10.1007/978-3-030-38509-5_9
- Beasley M. A., Bridges T., Peng E., Harris W. E., Harris G. L. H., Forbes D. A., Mackie G., 2008, *MNRAS*, **386**, 1443
- Beasley M. A., Fahrion K., Gvozdenko A., 2024, *MNRAS*, **527**, 5767
- Beasley M. A., Fahrion K., Guerra Arencibia S., Gvozdenko A., Montes M., 2025, *A&A*, **697**, A144
- Bottinelli L., Gouguenheim L., Paturel G., de Vaucouleurs G., 1984, *A&AS*, **56**, 381
- Bridges T. J., Hanes D. A., 1992, *AJ*, **103**, 800
- Bridges T. J., Ashman K. M., Zepf S. E., Carter D., Hanes D. A., Sharples R. M., Kavelaars J. J., 1997, *MNRAS*, **284**, 376
- Bridges T. J., Rhode K. L., Zepf S. E., Freeman K. C., 2007, *ApJ*, **658**, 980
- Brodie J. P., Strader J., 2006, *ARA&A*, **44**, 193
- Caldwell N., Schiavon R., Morrison H., Rose J. A., Harding P., 2011, *AJ*, **141**, 61
- Cappellari M., 2017, *MNRAS*, **466**, 798
- Cappellari M., 2023, *MNRAS*, **526**, 3273
- Cappellari M., Emsellem E., 2004, *PASP*, **116**, 138
- Carretta E., Gratton R. G., Clementini G., Fusi Pecci F., 2000, *ApJ*, **533**, 215
- Ciardullo R., Jacoby G. H., Tonry J. L., 1993, *ApJ*, **419**, 479
- Coelho P. R. T., 2014, *MNRAS*, **440**, 1027
- Cohen R. E., Goudfrooij P., Correnti M., Gnedin O. Y., Harris W. E., Chandar R., Puzia T. H., Sánchez-Janssen R., 2020, *ApJ*, **890**, 52
- Djorgovski S., 1995, *ApJ*, **438**, L29
- Dowell J. L., Rhode K. L., Bridges T. J., Zepf S. E., Gebhardt K., Freeman K. C., de Boer E. W., 2014, *AJ*, **147**, 150
- Dumont A., et al., 2022, *ApJ*, **929**, 147
- Emsellem E., 1995, *A&A*, **303**, 673
- Faber S. M., Jackson R. E., 1976, *ApJ*, **204**, 668
- Fahrion K., Beasley M. A., Emsellem E., Gvozdenko A., Müller O., Rejkuba M., 2025, *arXiv e-prints*, p. arXiv:2508.10100

³ <http://www.astropy.org>

- Ferrarese L., et al., 2000, *ApJ*, 529, 745
- Forbes D. A., Grillmair C. J., Smith R. C., 1997, *AJ*, 113, 1648
- Ford H. C., Hui X., Ciardullo R., Jacoby G. H., Freeman K. C., 1996, *ApJ*, 458, 455
- Foreman-Mackey D., Hogg D. W., Lang D., Goodman J., 2013, *PASP*, 125, 306
- Gadotti D. A., Sánchez-Janssen R., 2012, *MNRAS*, 423, 877
- Harris W. E., Harris H. C., Harris G. L. H., 1984, *AJ*, 89, 216
- Harris W. E., Spitler L. R., Forbes D. A., Bailin J., 2010, *MNRAS*, 401, 1965
- Hau G. K. T., Spitler L. R., Forbes D. A., Proctor R. N., Strader J., Mendel J. T., Brodie J. P., Harris W. E., 2009, *MNRAS*, 394, L97
- Husser T. O., Wende-von Berg S., Dreizler S., Homeier D., Reiners A., Barman T., Hauschildt P. H., 2013, *A&A*, 553, A6
- Jardel J. R., et al., 2011, *ApJ*, 739, 21
- Jensen J. B., Tonry J. L., Barris B. J., Thompson R. I., Liu M. C., Rieke M. J., Ajhar E. A., Blakeslee J. P., 2003, *ApJ*, 583, 712
- Jensen J. B., Blakeslee J. P., Cantiello M., Cowles M., Anand G. S., Tully R. B., Kourkchi E., Raimondo G., 2025, *ApJ*, 987, 87
- Kang J., Lee M. G., Jang I. S., Ko Y., Sohn J., Hwang N., Park B.-G., 2022, *ApJ*, 939, 74
- Karunakaran A., Spekkens K., Zaritsky D., Donnerstein R. L., Kadowaki J., Dey A., 2020, *ApJ*, 902, 39
- Larsen S. S., Brodie J. P., Beasley M. A., Forbes D. A., 2002, *AJ*, 124, 828
- Masters K. L., et al., 2010, *ApJ*, 715, 1419
- McLaughlin D. E., 2000, *ApJ*, 539, 618
- McQuinn K. B. W., Skillman E. D., Dolphin A. E., Berg D., Kennicutt R., 2016, *AJ*, 152, 144
- Mieske S., et al., 2008, *A&A*, 487, 921
- Paturel G., Garnier R., 1992, *A&A*, 254, 93
- Pryor C., Meylan G., 1993, in Djorgovski S. G., Meylan G., eds, *Astronomical Society of the Pacific Conference Series Vol. 50, Structure and Dynamics of Globular Clusters*. p. 357
- Rejkuba M., Dubath P., Minniti D., Meylan G., 2007, *A&A*, 469, 147
- Rhode K. L., Zepf S. E., 2004, *AJ*, 127, 302
- Rizzi L., Tully R. B., Makarov D., Makarova L., Dolphin A. E., Sakai S., Shaya E. J., 2007, *ApJ*, 661, 815
- STScI Development Team 2018, synphot: Synthetic photometry using Astropy, Astrophysics Source Code Library, record ascl:1811.001
- Sabbi E., et al., 2018, *ApJS*, 235, 23
- Sorce J. G., Tully R. B., Courtois H. M., Jarrett T. H., Neill J. D., Shaya E. J., 2014, *MNRAS*, 444, 527
- Spitler L. R., Larsen S. S., Strader J., Brodie J. P., Forbes D. A., Beasley M. A., 2006, *AJ*, 132, 1593
- Strader J., Smith G. H., Larsen S., Brodie J. P., Huchra J. P., 2009, *AJ*, 138, 547
- Strader J., Caldwell N., Seth A. C., 2011, *AJ*, 142, 8
- Tonry J. L., Dressler A., Blakeslee J. P., Ajhar E. A., Fletcher A. B., Luppino G. A., Metzger M. R., Moore C. B., 2001, *ApJ*, 546, 681
- Tully R. B., Fisher J. R., 1988, *Catalog of Nearby Galaxies*
- Vazdekis A., Sánchez-Blázquez P., Falcón-Barroso J., Cenarro A. J., Beasley M. A., Cardiel N., Gorgas J., Peletier R. F., 2010, *MNRAS*, 404, 1639
- Vazdekis A., Koleva M., Ricciardelli E., Röck B., Falcón-Barroso J., 2016, *MNRAS*, 463, 3409
- Villegas D., et al., 2010, *ApJ*, 717, 603
- Wakamatsu K. I., 1977, *PASP*, 89, 267

APPENDIX

TABLE OF DISPERSION MEASUREMENTS

We report the velocity dispersions, magnitudes, and where available sizes and mass-to-light ratios in Table 3. The identifiers refer to the catalogue presented in Fahrion et al. (2025).

This paper was built using the Open Journal of Astrophysics L^AT_EX template. The OJA is a journal which provides fast and easy peer review for new papers in the astro-ph section of the arXiv, making the reviewing process simpler for authors and referees alike. Learn more at <http://astro.theoj.org>.

TABLE 3
DISPERSION MEASUREMENTS.

ID	RA (J2000)	DEC (J2000)	σ (km s ⁻¹)	r_h (arcsec)	$V_{\text{Spitler+2006}}$ (mag)	$V_{\text{Harris+2010}}$ (mag)	$V_{\text{Rhode\&Zepf2004}}$ (mag)	M_{dyn}/L_V (M_{\odot}/L_{\odot})
12 (SUCD1)	190.01304	-11.66786	26.55 ^{+0.35} _{-0.32}	0.34	...	17.46 ¹	...	3.38±0.33
13	190.03900	-11.64231	25.49 ^{+0.70} _{-0.61}	0.12	18.91	18.87	...	3.93±0.21
14	190.04279	-11.57125	10.62 ^{+2.28} _{-1.80}	0.07	20.11	20.07	20.14	1.16±0.47
15	190.04479	-11.78836	8.47 ^{+1.75} _{-1.81}	21.29	...
16	190.04667	-11.50436	6.52 ^{+2.42} _{-2.17}	21.21	...
17	190.04687	-11.84981	11.44 ^{+3.11} _{-2.78}	20.50	...
18	190.05292	-11.40906	6.66 ^{+2.65} _{-3.10}	21.53	...
19	190.03271	-11.38036	8.71 ^{+1.97} _{-1.84}	21.04	...
20	190.05500	-11.28775	13.03 ^{+1.69} _{-1.78}
21	190.07171	-11.95222	12.04 ^{+2.10} _{-2.10}
23	190.09050	-11.81750	5.79 ^{+1.26} _{-1.72}
24	190.09571	-11.79056	4.45 ^{+3.76} _{-4.37}	20.93	...
25	190.13242	-11.93833	7.78 ^{+2.07} _{-1.99}
26	190.06908	-11.55500	12.86 ^{+3.02} _{-2.03}	21.18	...
27	190.03042	-11.43528	11.36 ^{+3.58} _{-5.45}	20.88	...
28	190.02520	-11.59367	14.83 ^{+1.67} _{-1.60}	0.06	20.44	20.53	20.55	3.14±0.71
29	189.93025	-11.81147	7.67 ^{+2.49} _{-2.46}	20.85	...
30	189.95262	-11.59462	21.37 ^{+0.64} _{-0.60}	0.10	19.09	19.04	...	2.71±0.17
33	189.97587	-11.57515	16.34 ^{+1.06} _{-1.52}	0.11	19.93	19.80	19.83	3.60±0.57
34	189.97846	-11.68622	7.82 ^{+6.88} _{-6.61}
35	189.98367	-11.71906	14.34 ^{+3.75} _{-4.29}	20.98	...
36	190.02600	-11.85794	11.58 ^{+2.18} _{-1.76}	20.57	...
37	189.98450	-11.53192	20.08 ^{+0.39} _{-0.49}
39	190.02096	-11.48725	12.25 ^{+1.98} _{-1.94}	21.00	...
40	190.02262	-11.93269	5.30 ^{+2.10} _{-3.76}
41	190.02500	-11.49014	4.85 ^{+3.16} _{-4.81}	21.35	...
42	189.98825	-11.92911	5.06 ^{+3.03} _{-4.48}
75	189.98917	-11.64292	11.45 ^{+0.74} _{-0.80}
91	189.99075	-11.60258	18.04 ^{+0.80} _{-1.19}	0.07	19.39	19.36	...	1.77±0.21
134	190.16358	-11.75308	7.64 ^{+2.57} _{-3.05}	20.70	...
135	190.16233	-11.91731	17.75 ^{+0.75} _{-0.97}	19.68	...
136	190.15450	-11.76708	12.57 ^{+0.92} _{-0.72}	19.29	...
137	190.15421	-11.49092	18.57 ^{+1.27} _{-1.56}	19.44	...
139	190.15133	-11.68289	8.38 ^{+2.05} _{-1.39}	20.37	...
143	190.14529	-11.47961	17.73 ^{+1.47} _{-1.57}	20.02	...
145	190.14083	-11.75581	16.35 ^{+1.58} _{-1.45}	20.45	...
154	190.11308	-11.47386	8.93 ^{+1.12} _{-1.10}	20.68	...
160	190.10167	-11.89797	6.06 ^{+2.47} _{-2.96}	21.06	...
168	190.07933	-11.39892	11.79 ^{+1.82} _{-1.78}	20.25	...
172	190.07371	-11.67914	11.92 ^{+2.26} _{-2.95}	20.23	...
181	190.06475	-11.60589	6.42 ^{+1.53} _{-1.91}	0.08	20.21	20.18	20.19	0.61±0.33
182	190.06408	-11.62633	9.33 ^{+1.15} _{-1.00}	0.11	20.76	20.79	20.62	2.95±0.80
184	190.06367	-11.67028	22.88 ^{+0.64} _{-0.79}	0.08	19.37	19.38	19.33	3.58±0.23
189	190.06083	-11.53214	16.42 ^{+0.75} _{-0.96}	19.48	...
192	190.05729	-11.61739	19.69 ^{+1.65} _{-1.53}	0.04	19.80	19.89	19.91	2.08±0.34
194	190.05654	-11.65957	14.81 ^{+1.24} _{-1.27}	0.07	19.77	19.77	19.79	1.76±0.32
198	190.05179	-11.42597	11.20 ^{+0.72} _{-0.83}	19.55	...
210	190.04362	-11.75575	14.95 ^{+1.09} _{-1.04}	20.31	...
211	190.04333	-11.61078	19.39 ^{+0.70} _{-0.74}	0.08	19.02	18.99	18.98	1.79±0.14
215	190.04037	-11.60633	15.68 ^{+0.86} _{-0.72}	0.09	19.57	19.43	19.45	1.86±0.20
218	190.03883	-11.58786	21.36 ^{+1.02} _{-1.51}	0.06	19.75	19.83	19.85	3.51±0.43
221	190.03587	-11.65861	14.74 ^{+0.86} _{-0.72}	0.09	19.94	19.92	19.85	2.66±0.32

¹ Magnitude of SUCD1 reported in [Hau et al. \(2009\)](#). ID refers to the ID in the catalogue of [Fahrion et al. \(2025\)](#). Velocity dispersions after aperture correction.

ID	RA (J2000)	DEC (J2000)	σ (km s ⁻¹)	R_h (arcsec)	$V_{\text{Spitler+2006}}$ (mag)	$V_{\text{Harris+2010}}$ (mag)	$V_{\text{Rhode\&Zepf2004}}$ (mag)	M_{dyn}/L_V (M_{\odot}/L_{\odot})
222	190.03537	-11.72353	11.69 ^{+1.46} _{-1.44}	20.38	...
226	190.03179	-11.76808	14.54 ^{+1.30} _{-1.31}	20.02	...
231	190.02949	-11.60131	13.67 ^{+0.56} _{-0.73}	0.10	19.79	19.79	19.67	2.26±0.22
239	190.02342	-11.54158	18.94 ^{+3.34} _{-3.76}	20.38	...
240	190.02275	-11.43819	15.90 ^{+1.51} _{-1.10}	20.06	...
248	190.01504	-11.48775	4.43 ^{+3.03} _{-4.39}	21.39	...
249	190.01500	-11.54497	10.72 ^{+0.84} _{-0.86}	20.48	...
255	190.00900	-11.50750	13.70 ^{+0.82} _{-0.79}	19.87	...
264	190.00225	-11.74897	15.77 ^{+0.59} _{-0.51}	19.77	...
276	189.99562	-11.58962	16.86 ^{+0.83} _{-0.79}	0.08	19.51	19.49	19.53	2.01±0.20
279	189.99167	-11.57417	13.90 ^{+0.89} _{-0.90}	0.06	20.20	20.27	20.28	2.24±0.29
281	189.98996	-11.52369	16.43 ^{+0.44} _{-0.43}	19.28	...
283	189.98700	-11.33994	9.56 ^{+1.69} _{-1.60}	20.25	...
288	189.98400	-11.76928	12.17 ^{+1.89} _{-1.91}	20.31	...
292	189.98221	-11.65899	11.93 ^{+0.83} _{-0.63}	0.08	20.32	20.30	20.30	2.33±0.29
293	189.98083	-11.55678	15.99 ^{+0.73} _{-0.81}	19.81	...
302	189.97129	-11.85125	8.16 ^{+0.86} _{-1.24}	20.66	...
308	189.96717	-11.63383	16.73 ^{+1.33} _{-1.35}	0.06	20.23	20.27	20.29	3.11±0.52
320	189.96316	-11.64266	14.17 ^{+0.57} _{-0.63}	0.11	19.92	19.96	19.70	3.23±0.32
339	189.94404	-11.61414	14.92 ^{+0.44} _{-0.46}	0.10	19.84	19.82	19.68	2.81±0.32
340	189.94371	-11.58261	13.79 ^{+1.26} _{-1.02}	19.88	...
346	189.93874	-11.60014	19.00 ^{+0.50} _{-0.72}	0.13	19.33	19.28	19.13	3.67±0.26
355	189.92792	-11.71342	9.67 ^{+1.54} _{-1.63}	20.38	...
376	189.90033	-11.56905	13.20 ^{+2.35} _{-3.30}	20.65	...
378	189.89896	-11.79611	10.71 ^{+2.35} _{-2.27}	20.61	...
381	189.89629	-11.86453	14.19 ^{+0.95} _{-1.01}	19.98	...
382	189.89621	-11.50647	4.73 ^{+4.42} _{-4.69}	21.66	...
387	189.88625	-11.50875	9.04 ^{+1.37} _{-1.24}	20.18	...
395	189.87221	-11.49267	16.12 ^{+1.27} _{-1.47}	19.65	...
412	190.04184	-11.63909	29.15 ^{+0.90} _{-0.92}	0.08	18.79	18.74	...	3.26±0.26
413	190.00021	-11.60261	22.64 ^{+0.63} _{-0.63}	0.09	18.94	18.83	...	2.20±0.30
414	190.06078	-11.64111	20.55 ^{+0.46} _{-0.36}	0.11	18.98	18.83	...	2.29±0.20
423	189.99700	-11.64114	16.56 ^{+1.30} _{-1.66}	0.04	20.20	20.29	...	1.97±0.40
424	189.96816	-11.64635	12.49 ^{+1.82} _{-1.49}	0.09	20.20	20.13	...	2.29±0.61
429	189.97517	-11.60142	13.28 ^{+1.38} _{-1.14}	0.07	20.44	20.48	...	2.82±0.73